JOURNAL OF APPLIED ELECTROCHEMISTRY **28** (1998) 999–1004

# Effect of sulfate and chloride ions on the electrochemical behavior of iron in aqueous phosphate solutions

GHOLAMREZA VATANKHAH, HUGUES MENARD

*Chemistry Department, Sherbrooke University, Sherbrooke (Québec), Canada J1K 2R1*

LOUIS BROSSARD

*Institut de recherche d'Hydro-Québec, 1800 Boul. Lionel-Boulet, Varennes (Québec) Canada J3X 1S1*

Received 4 November 1997; revised 10 April 1998

The electrochemical behavior of iron in aqueous phosphate solutions (0.005–0.1 M) of pH~8 at room temperature was investigated with an emphasis on the effect of chloride and /or sulfate ions on the initiation of the localized attack. Electrochemical techniques were complemented by SEM microscopy, FTIR, X-ray fluorescence analysis and ICP measurements. It has been shown that phosphate ions are very effective inhibitors against localized attack, and in the presence of sulfate ions still show an effect very similar to that of phosphate ions in the active–passive dissolution peak region.

Keywords: *iron*, *phosphate media*, *chloride*, *sulfate localised*, *attack*

## 1. Introduction

Phosphate ions are known as corrosion inhibitors for iron and its alloys [1–6]. Phosphate compounds are also used to generate conversion coatings on mild steel [7] to improve the corrosion protection performance of paints; the low solubility of phosphate compounds induces the precipitations of such compounds on the metal surface. In previous work, the effect of sulfate ions on the electrochemical processes of iron electrodes in the presence of bicarbonate ions was investigated [8]; it was determined that the formation of green rusts played a key role in the passivation and pitting initiation processes.

Armstrong et al. [4] have reported that the addition of sodium phosphate up to 10 mM in aqueous solutions of carbonate and acetate buffers does not have any effect on the electrochemical behavior of iron in such solutions, whether aerated or deaerated. They have discussed the inhibitive effect of phosphate ions based on buffered and unbuffered solutions and concluded that phosphate ions have an inhibitive effect in unbuffered solutions. However, their unbuffered solution contained perchlorate ions, which are usually used as accelerators in phosphating baths and have an oxidizing effect to help phosphate ions protect the iron surface.

Oxide films formed on iron in phosphate solutions are characterized by the incorporation of phosphate ions into the film [10–14]; phosphate ions can block the film defects with a beneficial influence on the protection against further dissolution [14].

Benzakour and Derja [3] have established that the passivation process of iron in aqueous phosphate solutions is due to the formation of a precipitate layer instead of direct phosphate formation (solid state process). The electrodissolution in the passivity range is limited by the diffusion of phosphate ions towards the interface which is caused by the precipitation of the oxidized iron species.

Burstein and Davies [6] have studied the behavior of scratched iron electrodes (bare metal surface) in solutions containing chloride, phosphate and bicarbonate ions. It has been deduced that bicarbonate ions do not react directly with the bare metal surface while chloride and phosphate ions react directly with the bare metal surface to form FeCl and $FeH_2PO_4$. For metal surfaces covered with an oxide film, there is no direct contact between metal surface and electrolyte solution, and anodic oxidation occurs across the metal/film interface.

The present paper investigates the passivating effect of phosphate ions on iron at ambient temperature with an emphasis on the aggressive effects of sulfate and chloride ions both alone and together. The phosphate ion concentration ranges from 0.005 to 0.1 M, sulfate ion from 0.1 to 0.5 M, and chloride ion from 0.01 to 0.02 M.

## 2. Experimental details

The working electrodes were made of iron (Johnson Matthey) in a Kel-F holder used as a rotating-disk electrode. The exposed area was 0.13 $cm^2$. The electrodes were mechanically polished with alumina paste to a mirror-like finish and rinsed with distilled water. The electrode surface was examined before and after the experiments using a Bausch and Lomb optical microscope (70×). For each experiment, the electrode was kept at a constant applied potential of −1.0 V(sce) for one minute in order to reduce (as much as possible) air-formed surface oxides. The

auxiliary electrode was a platinum grid, which was separated from the main compartment by a Nafion® membrane. The reference electrode was a saturated calomel electrode (sce) with a Luggin capillary bridge connected to the main cell. All potentials in this paper are reported against the sce. The rotation speed ($\omega$) of the working electrode was typically 1000 rpm.

Aqueous solutions of 0.1–0.5 M $Na_2SO_4$ and 0.005–0.1 M $Na_2HPO_4$ plus 0.01–0.02 M NaCl were prepared from analytical grade materials (BDH) and deionized water. The pH was ~8 for all solutions and the pH was not adjusted during the course of the measurements. A ~600 mL cell was used to minimize the enrichment of the solution in dissolved ions during the experiments. All solutions were deaerated by high-purity nitrogen bubbling before each experiment and were purged continuously during the measurements. All of the experiments were carried out at room temperature.

The instrument used was a Potentiostat/Galvanostat model 273 from Princeton Applied Research (PAR) controlled by a PC using M270 PAR electrochemical software (version 4.10). Electrode rotation was achieved using an electrode rotator from the Pine Instrument Company.

## 3. Results

Figure 1 shows a potentiodynamic curve of an iron electrode rotated at 1000 rpm in 0.01 M $Na_2HPO_4$ (pH ~8) solution with a potential scan rate of 0.005 V $s^{-1}$ and potential limits of −0.84 and 2.0 V. The curve displays a dominant anodic peak current located at −0.6 V, its maximum current being ~90 $\mu A\,cm^{-2}$. The peak current is ascribed to a dissolution-passivation process, which is common for buffer inhibitors [15]. The peak current is followed by a large passive region extending from −0.4 V to +0.85 V. For E > 0.85 V, the transpassive region is observed where the more anodic the applied potential, the larger the current density due to the onset of oxygen evolution; no waves associated with ferrate species are noted as reported for bicarbonate aqueous solutions [8]. The potentiodynamic trace of the negative potential scan is characterized by a small cathodic peak at −0.6 V.

The potentiodynamic behavior of a rotating iron disk electrode is different in the presence of 0.01 M $Na_2HPO_4$ + 0.1 M $Na_2SO_4$ solution (Fig. 2), the potential scan rate and the limits being the same as those of Fig. 1: (i) the height and location of the first anodic peak (peak I) is practically the same for both solutions; (ii) a second anodic peak (peak II) close to 0.22 V is noted with some current oscillations in the presence of sulfate ions; (iii) a repassivation region extending from 0.5 V to 0.9 V with some current oscillations is observed in the presence of sulfate ions; (iv) at potentials higher than 1.0 V, a transpassive region with a small plateau current prior to the onset of the oxygen evolution reaction appears in the presence of sulfate ions. The small plateau current is absent on the potentiodynamic curve of iron when recorded in separate solutions of phosphate and sulfate ions, indicating that there is a synergetic effect of phosphate and sulfate ions when they are together in solution. The electrooxidation current remains non-negligible during the return sweep from 0.9 V to −0.2 V with a broad cathodic wave current at −0.6 V. The small anodic current oscillations in the region of anodic peak current II are ascribed to the metastable pitting induced by the presence of sulfate ions in the phosphate solution.

For a constant phosphate ion concentration, the higher the sulfate ion concentration, the greater the height of both peaks I and II and the lower the plateau current in the transpassive region (Fig. 3). The location of the two oxidation peaks is practically the same in 0.01 M $Na_2HPO_4$ + 0.1 to 0.5 M $Na_2SO_4$. The larger the phosphate ion concentration, the concentration in sulfate ions being constant, the lower the anodic current peaks I and II (Fig. 4). Peak II is accompanied by pitting corrosion in the presence of sulfate ions. The formation of a white precipitate as a corrosion product is observed at the pit sites.

The solution containing 0.01 M $Na_2HPO_4$ + 0.1 M $Na_2SO_4$ (Fig. 2) has been further considered to establish the effect of the anodic potential reversal on the potentiodynamic curves during the return sweep.

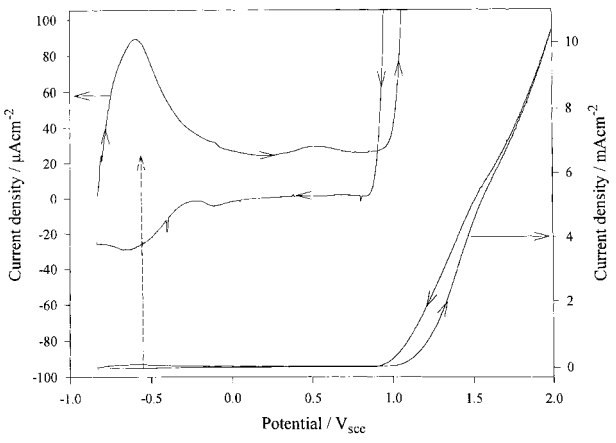


Fig. 1. Potentiodynamic trace for a rotating iron disk electrode, in 0.01 M sodium phosphate solution, dE/dt = 5 mV $s^{-1}$; $\omega$ = 1000 rpm. Starting potential: −0.84 V.

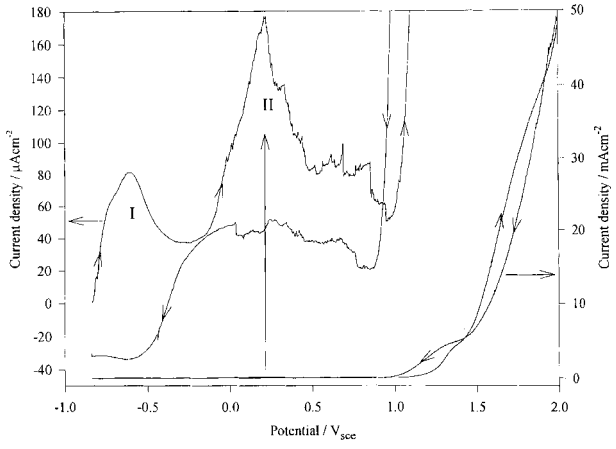


Fig. 2. Potentiodynamic trace for a rotating iron disk electrode, in 0.01 M sodium phosphate + 0.1 M sodium sulfate solution, dE/dt = 5 mV $s^{-1}$; $\omega$ = 1000 rpm. Starting potential: −0.84 V.

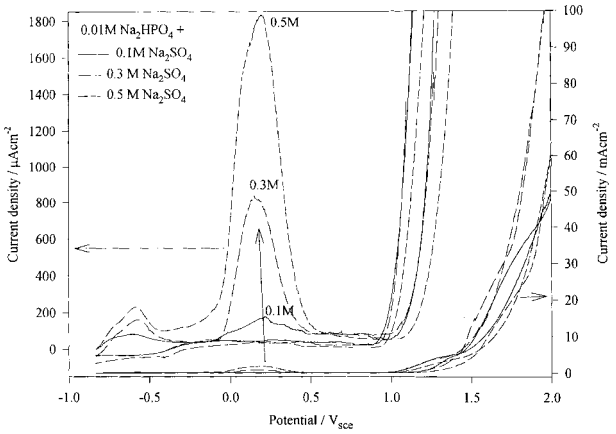


Fig. 3. Voltammograms for an iron electrode in 0.01 M phosphate + x M sulfate, x = 0.1, 0.3, and 0.5 M; $dE/dt = 5\ mV\ s^{-1}$; $\omega = 1000$ rpm; starting potential: −0.84 V.

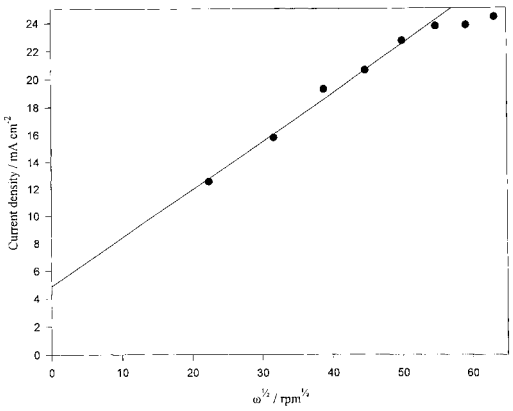


Fig. 5. Effect of electrode rotation speed on the electrooxidation steady-state current density at −0.6 V for an iron electrode in an aqueous solution of 0.1 M sulfate + 0.01 M phosphate. Current density after 20 min at a constant applied potential of −0.6 V was used as the steady-state value.

When the potential reversal is located in the region of pit initiation, i.e. the first part of peak II ($-0.1 < E < 0.2$ V), the current is larger during the return sweep due to pit growth. For the descending part of peak current II ($0.2 < E < 0.6$), the electrode surface is completely covered with corrosion products and the current during the return sweep is lower. As the anodic potential reversal becomes more anodic than ~0.5 V, the passivation range for the potential scan reversal is larger and the height of the cathodic peak current at −0.6 V increases.

The effect of $\omega$ on the steady-state electrodissolution current at −0.6 V (i.e. the maximum of current peak I) for $\omega$ ranging from 500 to 4000 rpm is illustrated in Fig. 5. The steady-state current has been attained after 20 min of polarization. A linear relationship is observed for the steady-state current density expressed against $\omega^{1/2}$ with $i \neq 0$ for $\omega \rightarrow 0$, $\omega$ being below 4000 rpm. It is deduced that the rate-determining-step of iron dissolution is mainly the diffusion of ionic species into the solution in the vicinity of the electrode surface. The effect of the potential scan rate (dE/dt) on the location of peak I and its height is illustrated in Fig. 6 for a stationary electrode in a quiescent solution. Again, it is deduced that diffusion of ionic species into the solution in the vicinity of the electrode surface plays a key role in limiting of the electrodissolution process involved in the region of peak I. As a first approximation, both peak current density and potential increase linearly with the square root of the scan rate, with a dissolution-precipitation mechanism being deduced [3]. For the electrodissolution current in the region of peak II, it is not possible to observe a steady-state value at a given $\omega$ (including $\omega = 0$) due to the stochastic nature of the pitting.

The current versus time curves recorded at constant applied potentials located in the region of peak II are characterized by a high oxidation charge before surface passivation as shown in Fig. 7 for an applied potential of 0.0 V (sce) ($Q_{ox} = 250\ C\ cm^{-2}$ after 8000 s). Chronoamperograms for constant applied potentials located in the ascending part of current peak II on the potentiodynamic curve have the following features: (i) for short times, the electrooxidation current increases with time to reach a maximum value which is very high; (ii) current oscillations are noted close to the current maximum and in the region where the current decreases with time. The current

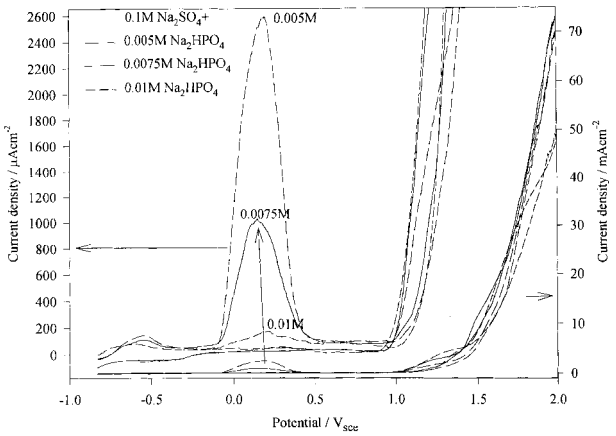


Fig. 4. Voltammograms for an iron electrode in 0.1 M sulfate + x M phosphate, x = 0.005, 0.0075, and 0.01 M; $dE/dt = 5\ mV\ s^{-1}$; $\omega = 1000$ rpm; starting potential: −0.84 V.

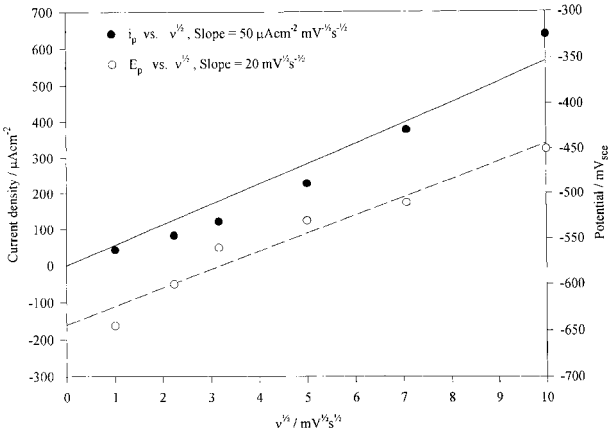


Fig. 6. $i_p$ and $E_p$ plotted against the square root of the potential sweep rate for an iron electrode in an aqueous solution of 0.1 M sulfate + 0.01 M phosphate. $\omega = 0$ rpm, sweep rate ranges from 1 to 100 $mV\ s^{-1}$.

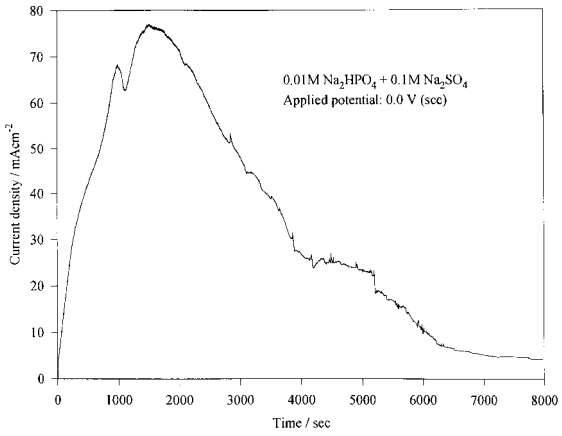


Fig. 7. Chronoamperogram for an iron electrode in a 0.1 M sulfate +0.01 M phosphate solution. $\omega$ =1000 rpm. Applied potential: 0.0 V (sce); $Q_{ox}$ = 250 C cm$^{-2}$.

oscillations are ascribed to a local film breakdown followed by a repair process. As the steady-state current was attained after several thousand seconds, the electrode surface was completely covered with a white precipitate which is poorly protective and adheres to the electrode surface. The precipitate was easily removed after each experiment and rinsed carefully with deionized water for further investigation. The ICP analysis, X-ray fluorescence analysis and FTIR spectroscopy were done for the precipitate obtained under different constant applied potentials located in the peak II region. The precipitate formed on the electrode surface in the solution is white but becomes green in contact with air. In spite of the 10:1 molar ratio of sulfate to phosphate ions in the solution, the precipitate contains mainly phosphate and a negligible amount of sulfate. FTIR spectra of the precipitate are in good agreement with the formation of iron phosphate (Fig. 8). From ICP measurements, a molar ratio Fe/P of 1.6 has been obtained for different constant applied potentials located in the peak II region; which is consistent with the formation of iron (II) phosphate. The same result was obtained with the X-ray fluorescence analysis, i.e. Fe/P = 3/2.

SEM pictures of the electrode surface after 1 min chronoamprometry at different applied potentials located in the peak II region were obtained (see Fig. 9 for an applied potential of 0.0 V). Shifting from E = −0.3 V to E = −0.2 V results in a larger localized attack. For 0.0 V ($Q_{ox}$ = 130 mC cm$^{-2}$), there is more pitting and more precipitate at the pit sites. The precipitate is amorphous. Stepping to more noble potentials, at E = 0.2 V ($Q_{ox}$ = 12 mC cm$^{-2}$), the pits decrease in number with less precipitate, and at E = 0.3 V ($Q_{ox}$ = 4 mC cm$^{-2}$) there is a further decrease in pits.

Figure 10 shows potential versus time curves recorded for different constant applied current densities ranging from 8 to 160 $\mu$A cm$^{-2}$. For applied current densities below 36 $\mu$A cm$^{-2}$, the potential quickly stabilizes in the region of peak I. For an applied current of 36 $\mu$A cm$^{-2}$, the potential is located in the peak I region up to 1500 s before its sudden increase in the transpassive region; this current is too low to initiate pitting under the experimental conditions of Fig. 10. For an applied current density larger than 36 $\mu$A cm$^{-2}$, the greater the current, the shorter the time during which the potential remains in the region of peak I. For 40 $\mu$A cm$^{-2}$, the potential jumps to −0.05 V after 800 s of polarization and pitting is ini-

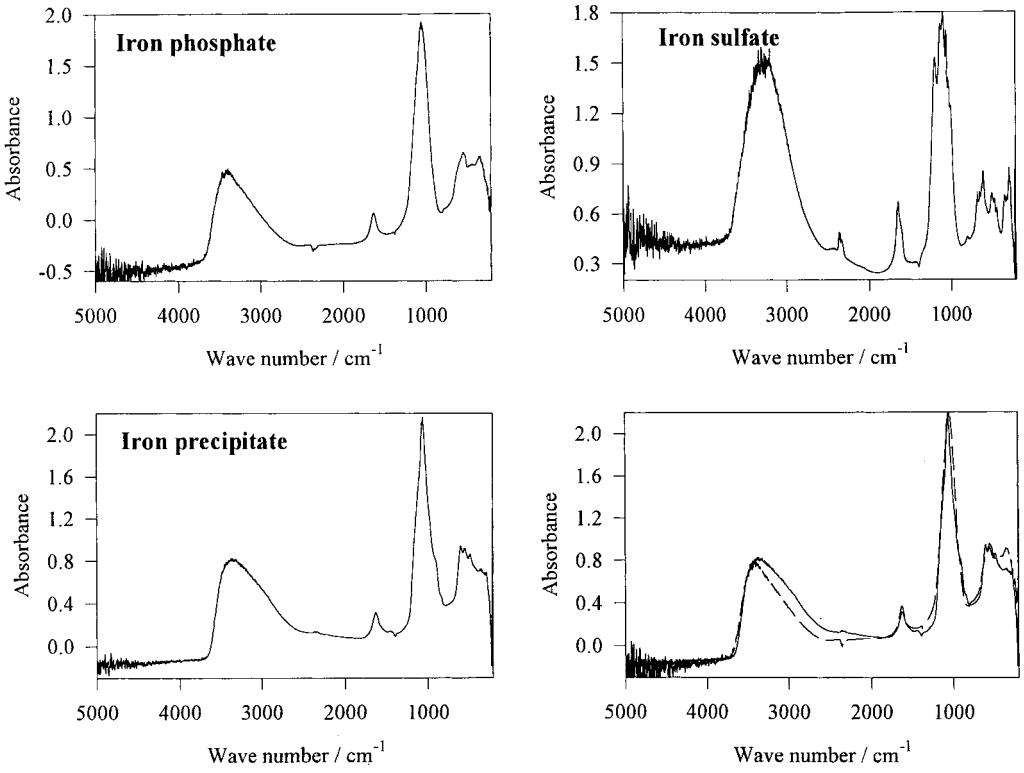


Fig. 8. FTIR spectra of the precipitate after formation under the experimental conditions of Fig. 7. Spectra for iron phosphate and sulfate.

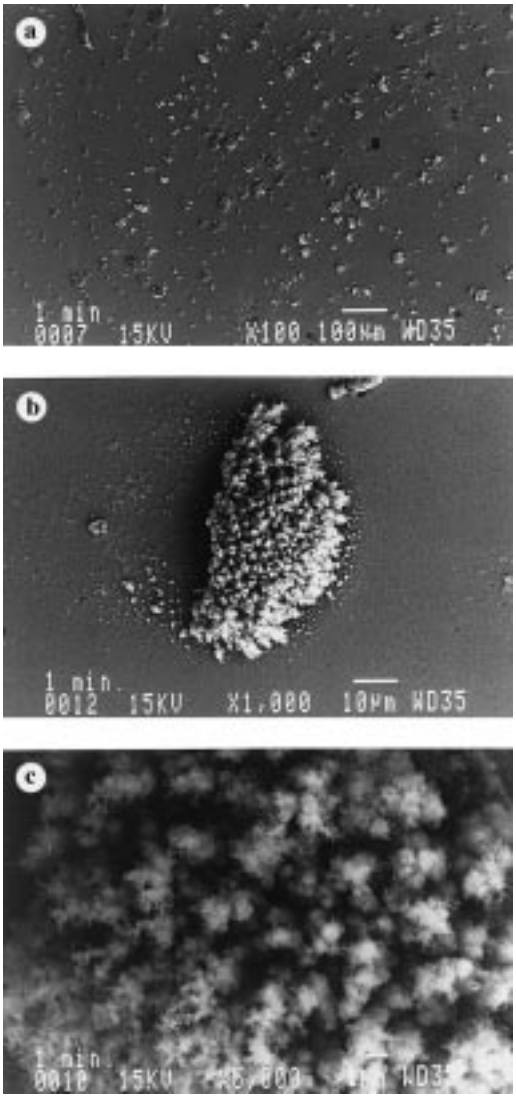


Fig. 9. SEM pictures (magnifications: x100, x1000, and x5000) after iron electrode oxidation at 0.0 V for 60 s in 0.1 M sodium sulfate + 0.01 M sodium phosphate solution; $\omega = 1000$ rpm; $Q_{ox} = 130$ mC cm$^{-2}$.

tiated; a potential drop is further noted before potential stabilization at $\sim -0.3$ V, i.e. in the region of peak II (Fig. 2); pit growth is observed. The picture is different for 48 $\mu$A cm$^{-2}$: after 500 s, the potential starts to shift in the positive potential direction and, at 0.1 V, the pitting process is noticed for a short time only before the potential shifts in the transpassive region. For an applied current density larger than 48 $\mu$A cm$^{-2}$, the greater the applied current density, the shorter the time to reach the transpassive region and no pits are formed.

Figure 11 shows the effect of the chloride ions on the potentiodynamic curve for iron electrodes in a solution containing 0.1 M $Na_2PO_4$ + 0.01 M and 0.02 M NaCl. Iron electrodes were rotated at 1000 rpm and the potential scan rate was 0.005 V s$^{-1}$ from −0.84 V to 2.0 V. The anodic current for the iron electrode in both solutions starts to increase at −0.84 V to reach a maximum of 100 $\mu$A cm$^{-2}$ at E = −0.7 V. This behavior is related to a dissolution-passivation mechanism. The peak current is followed by a large passive region ranging from −0.4 V to 0.9 V; for E > 0.9 V, the more anodic the applied potential, the greater the current density due to the onset of the oxygen evolution. No waves resulting from ferrate ion formation are observed in the transpassive region. Some pits are initiated in the transpassive region and further grow as the potential is swept in the negative direction; green corrosion products cover the pit sites during pit growth. The reminder of the electrode surface is untouched and looks shiny. The effect of the anodic potential reversal has been investigated for $E_a$ of 1.0 and 1.5 V to demonstrate the absence of any pit initiation. Hence, it is at more anodic potentials located in the transpassive region that pits can initiate in the case of low chloride ion concentrations. Fig. 11 also shows that the higher the concentration of chloride ions, the greater the associated current density, the larger the amplitude and the higher the frequency of the current oscillations for the potentiodynamic curve in the anodic potential direction.

## 4. Discussion and conclusions

The electrochemical behavior of iron electrodes in sulfate aqueous solutions has been reported in a

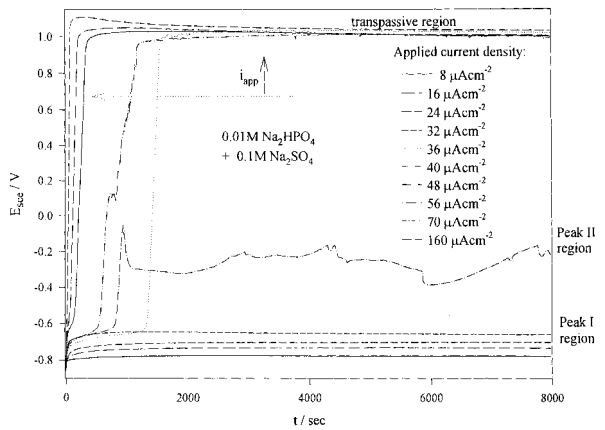


Fig. 10. Chronopotentiograms for an iron electrode in a 0.1 M sulfate + 0.01 M phosphate solution. $\omega = 1000$ rpm. Applied current density from 8 to 160 $\mu$A cm$^{-2}$.

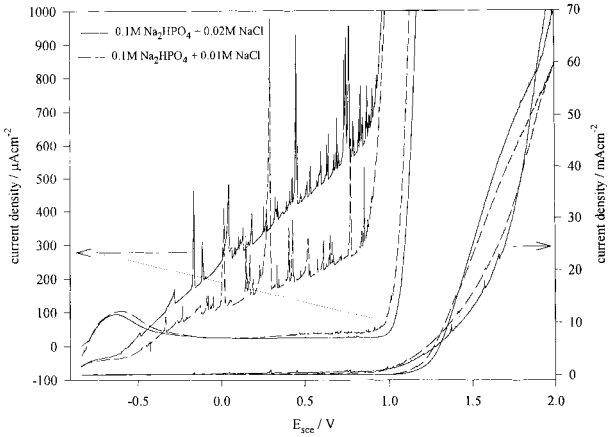


Fig. 11. Voltammograms for an iron electrode in 0.01 M phosphate + x M chloride, x = 0.01, and 0.02; dE/dt = 5 mV s$^{-1}$; $\omega = 1000$ rpm; starting potential: −0.84 V.

previous paper [8], where it was established that the dissolution process is uniform in the presence of sulfate ions. It has been pointed out that there is no wave related to ferrate ions formation for iron in inhibitor free solutions of sulfate ion (Fig. 1 in [7]). As far as the potentiodynamic characteristics of the iron electrode in phosphate solution are concerned (Fig. 1), passivation proceeds through a dissolution-precipitation mechanism when the potential is sufficiently anodic [3]. In aqueous sulfate solutions (Fig. 2), a second anodic current peak on the potentiodynamic trace is characterized by current oscillations with a small amplitude, the current oscillations being linked to pitting corrosion. The potentiodynamic trace also displays a small wave in the transpassive region which is characteristic of ferrate ion formation. Since the formation of ferrate ions is only noticed when both phosphate and sulfate ions are present together, it is deduced that the formation of ferrate is possible through a synergetic effect of sulfate and phosphate ions. The addition of more phosphate to sulfate solutions (Figs. 3 and 4) resulted in an increase of the peak I and a decrease of the peak current II. In solutions containing phosphate ions, it is relevant to consider the different species which can exist in solution as a function of pH [14]. During iron dissolution in the presence of sulfate ions, the surface pH can change by hydrolysis of iron species and, depending on the local pH attained in the vicinity of the electrode, stable species of phosphate can possibly affect the electrodissolution process. The anodic peaks I and II are most likely related to the formation of iron phosphate precipitates. For phosphate + sulfate solutions, and as far as peak I region is concerned (Figs. 5 and 6), a dissolution-precipitation mechanism mainly controlled by diffusion of ionic species into the solution in the vicinity of the electrode is deduced, as reported for the dissolution of iron in aqueous phosphate solutions [3]. It is concluded from FTIR spectra (Fig. 8) that the precipitate is iron phosphate. Chronoamperograms of iron electrodes at 0.0 V (Fig. 7) show how the current density increases with the dissolution of iron during pit initiation and growth. The pits are eventually covered with precipitates (Fig. 9) and current density consequently decreases with time.

Comparing the effect of chloride and sulfate ions on the electrooxidation behavior of the iron surface in the presence of phosphate solutions, it was observed that chloride ions are very aggressive compared to the sulfate ions. However, for potentials that are negative with respect to the transpassive region, there is a critical chloride ion concentration with respect to phosphate ions below which the rate of electrodissolution process is small and the electrode surface remains untouched. It is also interesting to note that the presence of chloride ions results in the formation of green rust 1 as a corrosion product during the course of pitting corrosion, the precipitate being white in the presence of sulfate ions and phosphate ions. The iron dissolution, with generation of ferrous ions within the pits, combined with the presence of phosphate ions, induces the precipitation of ferrous phosphate ($pK_{sp} = -32$ compared to $-26$ for ferric phosphate) [17] (Figs. 7–9). The possible existence of any rust arising from aqueous solutions of iron with both sulfate and phosphate ions, in contrast to sulfate and carbonate ions, remains an open question [16]. Hence, it has been concluded that the mechanism of passivation by phosphate ions and bicarbonate ions is different, and chloride ions always produce green rust 1 for both solutions.

In summary, the following features are characteristics for ion electrodissolution in solutions containing phosphate ions in the presence of sulfate or chloride ions: i) In phosphate solutions only, the passivation process proceeds through a dissolution-precipitation mechanism, ii) in solutions of phosphate + sulfate ions, the passivation process is unchanged from that arising in the presence of phosphate ions only; it is different from the one for sulfate solutions of bicarbonate, most likely because the low solubility of the phosphate precipitates affects their behavior, iii) in the presence of chloride ions, pitting corrosion goes through green rust 1 without any repassivation.

## Acknowledgements

Gh. Vatankhah gratefully acknowledges the Ministry of Culture and Higher Education (MCHE) of Iran for his graduate scholarship. The authors also acknowledge the financial support of Hydro-Québec (IREQ), the Natural Sciences and Engineering Research Council of Canada (NSERCC).

## References

[1] M. J. Pryor and M. Cohen, *J. Electrochem. Soc.* **98** (1951) 263.
[2] M. J. Pryor and M. Cohen, *J. Electrochem. Soc.* **99** (1951) 542.
[3] J. Benzakour and A. Derja, *Electrochimica Acta* **38** (1993) 2547.
[4] R. D. Armstrong, L. Peggs and A. Walsh, *J. Appl. Electrochemistry* **24** (1994) 1244.
[5] M. Cohen, *J. Electrochem. Soc.* **32** (1976) 461.
[6] G. T. Burstein and D. H. Davies, *Corrosion Sci.* **20** (1980) 1143.
[7] G. Górecki, *Corrosion* **48** (1992) 613.
[8] Gh. Vatankhah, M. Drogowska, L. Brossard and H. Menard, *J. Appl. Electrochemistry* **28** (1998) 173.
[9] Gösta Wranglén, *An Introduction to Corrosion and Protection of Metals*, Chapman and Hall, London, 1985.
[10] J. E. O. Mayne and J. W. Menter, *J. Chem. Soc.* (1954) 103.
[11] K. Tokunaga, *Japanese J. of Applied Physics*, **21** (1982) 1693.
[12] C. A. Melendres, N. Camillone III and T. Tipton *Electrochimica Acta*, **34** (1989) 281.
[13] K. Azumi, T. Ohtsuka and N. Sato, *J. Electrochem. Soc.* **134** (1987) 1352.
[14] J. B. Lumsden and Z. Szklarska-Smialowska, *Corrosion* **34** (1978) 169.
[15] R. P. Frankenthal and J. Krugger, Eds.; *Passivity of Metals*; The Electrochemical Society: Princeton, NJ, 1977.
[16] J. M. R. Genin, A. A. Olowe, Ph. Refait and L. Simon, *Corrosion Sci.* **38** (1996) 1751.
[17] W. Stumm and J. J. Morgan, *Aquatic Chemistry*, John Wiley and Sons, NY, 1996.